Fluid Phase Equilibria 518 (2020) 112625

Contents lists available at ScienceDirect

Fluid Phase Equilibria

journal homepage: www.elsevier.com/locate/fluid

A molecular dynamics simulation study of KF and NaF ion pairs in hydrothermal fluids

Xiaoyu Zhang , Xiandong Liu *, Mengjia He , Yingchun Zhang , Yicheng Sun , Xiancai Lu

State Key Laboratory for Mineral Deposits Research, School of Earth Sciences and Engineering, Nanjing University, Nanjing, 210093, PR China

ARTICLE INFO

Article history:
Received 27 November 2019
Received in revised form
19 April 2020
Accepted 24 April 2020
Available online 7 May 2020

Keywords:
Molecular dynamics
KF
NaF
Potentials of mean force
Association constants

ABSTRACT

Classical molecular dynamics (MD) simulations were performed to study the association of KF and NaF ion pairs in water in a wide range of temperatures (423–1273 K) and densities (0.10–0.60 g/cm^3). The association constants (K_A) derived from the potentials of mean force (PMF) exhibit a rising tendency as temperature increases or density decreases. The association of NaF is similar to KF under most conditions but evidently larger at higher temperatures and lower densities. The radial distribution function (RDF) and coordination number (CN) reveal the characteristics of ion-water microstructures. There is significant water clustering near the K^+/Na^+ at high temperatures or low densities. The results indicate that fluoride ion acts as an important ligand complexing with K^+/Na^+ and promotes their migration and concentration in hydrothermal fluids.

1. Introduction

Fluorine is a common halogen group element in geo-fluids and it plays important roles in the process of mineralization [1–5]. Many types of deposits, including Iron Oxide-Copper-Gold (IOCG), Iron Oxide-Apatite (IOA), Tin, and REE deposits, are found to have high concentration of fluorine [6–11]. In hydrothermal fluids, fluoride ions can form a series of complexes with many cations, such as Mg^{2+}, Fe^{3+}, Ca^{2+}, Al^{3+}, Na^+ and K^+. The complexation is considered as an important approach to aid the transportation of fluoride ions [12–14]. In geological environment, abundant Na^+ and K^+ contained in rock-forming minerals are important cations forming complexes with fluoride ions. Previous experimental observations also showed that fluorite is more soluble in solutions containing NaCl/KCl than pure water [15–17]. This phenomenon is attributed to the formation of fluoride complexes, which dramatically increase the solubility of fluorite, particularly at high temperatures [17]. In electrolyte solutions, the association of charged ions form the distinct chemical species known as ion pairs [18]. According to the number of layers of water molecules between charged ions, ion pairs can be divided into contact ion pair (CIP, contact directly), solvent shared ion pair (SIP, single solvent layer between two ions) and solvent separated ion pair (2SIP, double solvent layers between two ions). The molecular-level study of KF and NaF ion pairs in water is vital to understanding of the properties of fluoride complexes. Furthermore, elucidating thermodynamic behaviors of KF and NaF ion pairs at high temperatures is helpful for understanding the mobility and transport of F in geological fluids.

Experimentally, ion pair association constant (K_A) can be determined through conductivity or spectrophotometric measurements. Miller et al. reported the K_A values of NaF at the temperatures (288 K, 298 K and 308 K) in marine environment [19]. Manohar et al. and Usha et al. measured the K_A of KF and NaF at 298 K in a wide range of pressure (1–2000 atm) [20,21]. Franck et al. obtained the K_A values of NaF at 823 K and different water densities (0.30, 0.50 and 0.70 g/cm^3) [22]. Richardson et al. obtained the K_A values of NaF at the temperatures (473 K and 533 K) from curve fitting, but the densities were not mentioned [17]. Lukyanova et al. measured the K_A values of NaF at 298 K, 323 K and 348 K, respectively [23]. However, experimental K_A values of NaF and KF ion pairs at higher temperatures (above 823 K) are lacking. At different water densities, K_A values are incomplete due to the limits of experimental techniques. For the research in subduction zone and the lower crust, ion pair K_A values of KF/NaF are urgently needed [24], which is crucial for estimating the amounts of ion pairs relative to free ions in high-temperature geological fluids.

* Corresponding author.
E-mail address: xiandongliu@nju.edu.cn (X. Liu).

https://doi.org/10.1016/j.fluid.2020.112625
0378-3812/

Molecular dynamics (MD) simulation provides a new way to obtain K_A values of ion pairs. MD has been widely applied in the studies of LiCl, NaCl and KCl ion pairs at supercritical conditions, e.g., see [25–28] and references therein. Fennell et al. investigated ion pair interaction of alkali metal fluoride (Li^+, Na^+, K^+, Rb^+ and Cs^+/F^-) and calculated the corresponding association constants at ambient conditions [29]. However, K_A values of NaF/KF ion pairs have not been investigated by using MD at higher temperatures.

In this study, classical MD simulations have been employed to calculate the potential of mean force (PMF) and K_A values of NaF/KF ion pairs at high temperatures. The microstructures of ion pairs were characterized in detail by analyzing the MD trajectories. Ion pair K_A values were predicted at a series of temperatures. This study provides important data for future research on hydrothermal fluids, which is useful for understanding the transportation and complexation of fluoride ions with important metal ions in geo-fluids.

2. Methods

2.1. Model

One ion pair (K^+/Na^+-F^-) and water molecules were randomly inserted into a 3D periodic cubic cell. At the ambient conditions, MD simulation was performed at 298 K and 1.0 g/cm^3 with the system containing 500 water + 1 K/NaF. At the higher temperatures (423, 523, 653, 873 or 1273 K), a series of simulations were performed at different water densities (0.10, 0.30 and 0.60 g/cm^3) with the system of 250 water + 1 K/NaF. The side lengths of simulation box were calculated from the densities. The detailed parameters of the systems were provided in Table S1. The initial configurations were generated by using the Packmol package [30]. Additional simulations have been performed with systems (including 250 Water + 1NaF, 500 Water + 1NaF, 1000 Water + 1NaF) to examine the finite-size effects. As shown in Fig. S1, the differences of PMF profiles between the systems (250 Water + 1NaF, 500 Water + 1NaF) are small enough and the resulting log K_A(m) values are identical, proving that the systems of 250 Water + 1Na/KF are big enough for the simulations.

2.2. Classical molecular dynamics simulation

All MD simulations were carried out using the DL_POLY 4.09 package [31]. In this study, the SPC/E water model [32] was employed, which has been widely used in aqueous solution systems [33–36]. The previous studies have confirmed that SPC/E model describes well its liquid-vapor coexistence curve, provides better diffusive properties and reproduces good dielectric constants at supercritical conditions [37–39]. The potential models of Dang [40] and Smith and Dang [41] were used for K^+/Na^+ and F^- ions. The parameters were summarized in Table S2. As Chialvo mentioned [25], the Smith and Dang models are specially parametrized for SPC/E water model. Smith and Dang models with SPC/E water model have been successfully used for calculating properties of alkali metal halide in supercritical water [25–27]. The previous work [26] has confirmed that the derived association constants for NaCl ion pairs agree well with the experimental results at different densities within 1 log K_A unit at different densities (0.4 g/cm^3 and 0.7 g/cm^3).

The interaction potentials between water-ion and ion-ion consist of the Lennard-Jones (LJ) potential and Columbic term as described in expression (1)

$$\phi_{ij} = 4\varepsilon_{ij}\left[\left(\frac{\sigma_{ij}}{r_{ij}}\right)^{12} - \left(\frac{\sigma_{ij}}{r_{ij}}\right)^{6}\right] + \frac{q_i q_j}{r_{ij}} \quad (1)$$

where ϕ_{ij} is the potential energy between the atoms i and j with the distance r_{ij}. σ_{ij} and ε_{ij} are LJ parameters. q_i and q_j are the atomic charges. Herein, a cutoff radius of 10 Å was set for van der Waals interaction. Long-range Coulomb forces were handled using the Ewald sum method with a real-space cutoff of 10 Å and a precision of 1.0E-6. As shown in Fig. S2a, the resulting PMF with a larger cutoff of 20 Å is almost the same as that calculated with the cutoff of 10 Å. The calculated log K_A(m) values are 7.62 ± 0.14 (10 Å) versus 7.55 ± 0.15 (20 Å) indicating that the cutoff 10 Å is big enough for the simulations. A different Ewald precision (1E-8) was tested. As shown in Fig. S2b, the same PMF curve was obtained, indicating that 1E-6 is enough. The SHAKE algorithm was used with a tolerance of 1.0E-6 to fix the distance between Na^+/K^+ and F^- [42]. For the rotational motion of rigid-bodies of water, a quaternion approach was implemented with a tolerance of 1.0E-6 [43]. The crossing terms of LJ parameters were determined by applying Lorentz-Berthelot combining rules [44], that is, $\varepsilon_{ij} = \sqrt{\varepsilon_i \varepsilon_j}$ and $\sigma_{ij} = 1/2(\sigma_i + \sigma_j)$. The leapfrog algorithm with a time step of 1.0 fs was used to integrate the equations of motion. The temperature was maintained using the Nosé-Hoover chain thermostat [45,46]. For each system, the initial configuration was firstly equilibrated for 500.0 ps before the production run was carried out for 2.0 ns.

2.3. Potential of mean force (PMF) and association constant (K_A)

The average mean force values $f(r)$ at ion separation r were calculated using the method of constraint. In each constrained MD simulation, extra constraint was imposed to fix the two ions at a distance, ranging from 8.0 to 2.0 Å with a distance interval of 0.20 Å. The PMF $W(r)$, in equation (2), was obtained by integrating $f(r)$ with respect to r.

$$W(r) - W(r_0) = -\int_{r_0}^{r} f(r)dr \quad (2)$$

Here, r is the distance between the two ions and r_0 is the reference distance. In continuum water medium, the PMF at r_0, $W(r_0)$, was calculated from equation (3), which was regarded as effective potential at the reference position [26].

$$W(r_0) = -\frac{e^2}{4\pi\varepsilon r_0 \varepsilon_0} + 4\varepsilon_{LJ}\left[\left(\frac{\sigma_{LJ}}{r_0}\right)^{12} - \left(\frac{\sigma_{LJ}}{r_0}\right)^{6}\right] \quad (3)$$

ε_{LJ} and σ_{LJ} are the LJ parameters of K^+ and Na^+ listed in Table S2. ε_0 is vacuum permittivity. In this study, r_0 was set as 8.0 Å and ε is the relative dielectric constant of SPC/E water model [38], as listed in Table S3.

The ion-pair association constants K_A, under infinite dilution condition were calculated from the PMFs with equation (4) [25,47]:

$$K_A = 4\pi N_A 10^{-27} \int_0^{r_c} exp\left(-\frac{W(r)}{kT}\right) r^2 dr \quad (4)$$

where r_c is the cutoff distance distinguishing "free ions" and "associated ion pair". N_A is the Avogadro constant, k is the Boltzmann constant, and T is the target temperature. K_A (L mol^{-1}) was converted into the molarity based association constant $K_A(m)$ (kg mol^{-1}) by multiplying the fluid density ρ (g/cm^3),

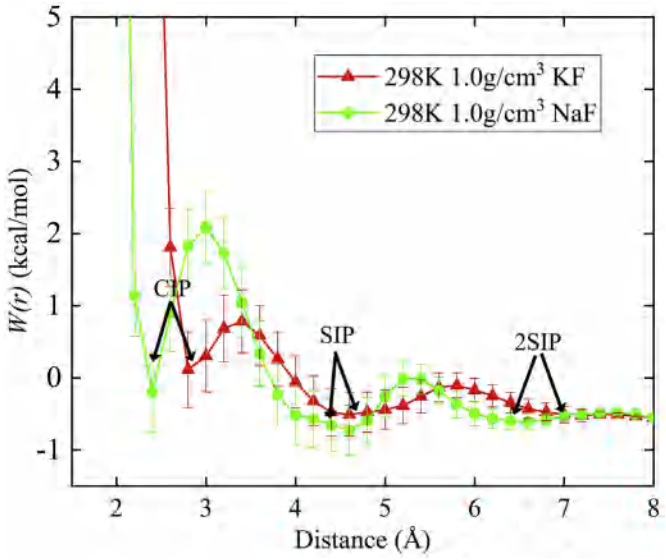

Fig. 1. PMFs of KF and NaF ion pairs at ambient conditions.

$$K_A(m) = K_A\rho \tag{5}$$

For the calculations of the errors in PMF and K_A, we firstly computed the standard deviations in forces (i.e. $f(r)$ in equation (2)). The errors in the PMFs were derived from the integration of the standard deviations in $f(r)$ according to equation (3). Then the errors in K_A were obtained by integrating the errors in the PMFs according to equation (4).

For the determination of r_c, there have been two different criterions, K_A for CIP or CIP + SIP, corresponding to the first and second maximum of relevant PMF curves. Some researchers calculated K_A values by taking only CIP as associated state at ambient conditions [48,49]. At high temperatures, more studies regarded both CIP and SIP as associated ion pair because the difference between the two criterions becomes smaller as temperature increases or solvent density decreases [25–28]. For instance, the calculated log K_A(m) values in this work for NaF ion pair at 423 K and 0.60 g/cm^3 showed that log K_A(m) of CIP + SIP is only 0.64 logarithm units higher than that of CIP. Hence in this paper, two criterions of r_c for CIP and CIP + SIP are adopted for the calculation of K_A(m) at ambient conditions, whereas only r_c for CIP + SIP are adopted to calculate the K_A(m) under high temperature conditions.

3. Results and discussions

3.1. Potential of mean force

At the ambient conditions, three types of ion pairs (CIP, SIP, 2SIP) were identified clearly on the PMF curves, which correspond to the positions of the first, second and third local minima, respectively (Fig. 1). Specific configurations at different associated states were carefully depicted by the snapshots of NaF/KF ion pairs at 298 K and 1.00 g/cm^3 (Fig. 2), which were obtained from the simulation trajectories. In Fig. 1, the calculated minima for NaF ion pair are located

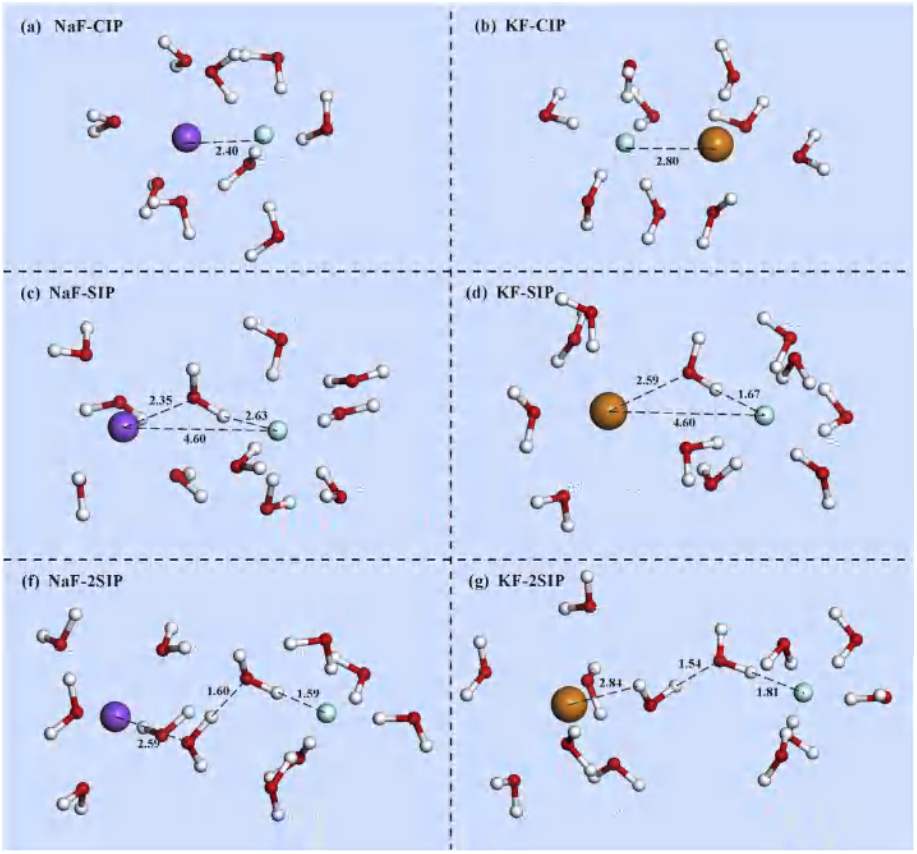

Fig. 2. Snapshots at CIP state **(a, b)**, SIP state **(c, d)** and 2SIP state **(e, f)** for NaF/KF ion pairs were obtained from constrained MD simulation at T = 298 K and ρ = 1.00 g/cm^3. For clarity, only ions and neighboring water molecules are displayed by ball and stick model. Hydrogen bonding is marked with blue dashed lines. Red = oxygen, white = hydrogen, purple = sodium, orange = potassium and cyan = fluorine.

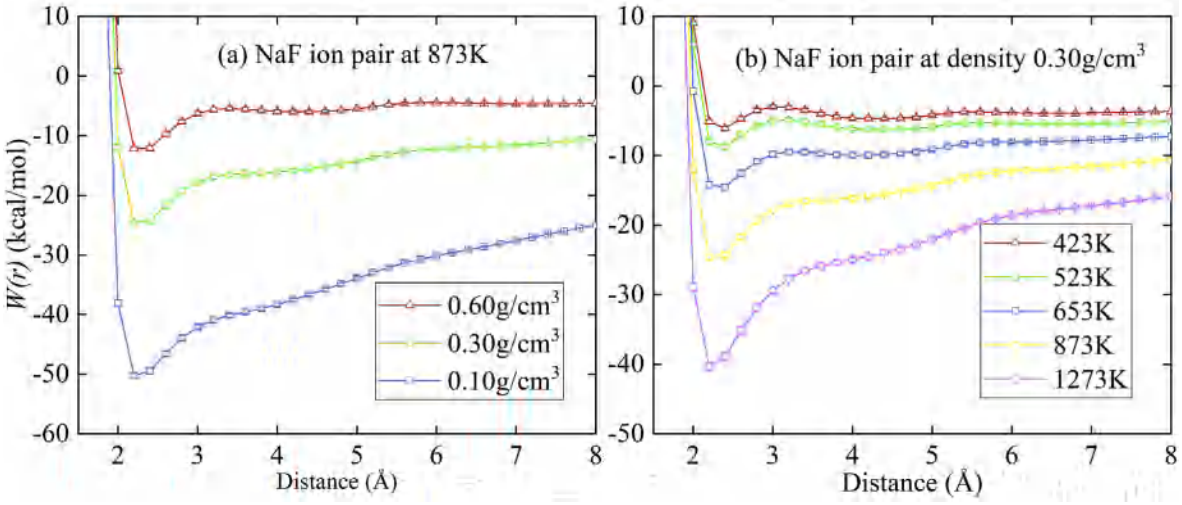

Fig. 3. The temperature dependence (**a**) and density dependence (**b**) of NaF PMF curves.

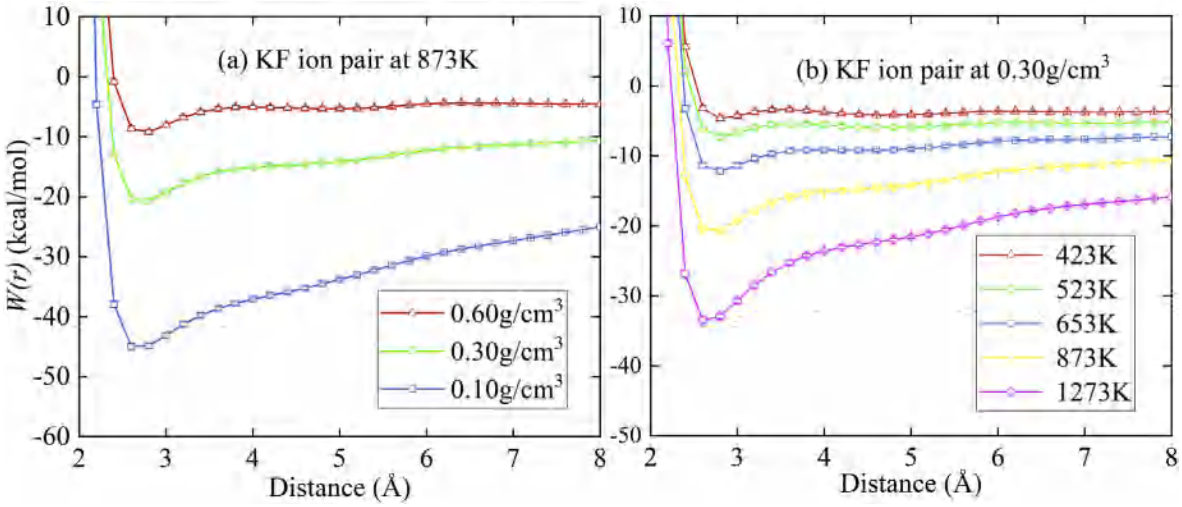

Fig. 4. The temperature dependence (**a**) and density dependence (**b**) of KF PMF curves.

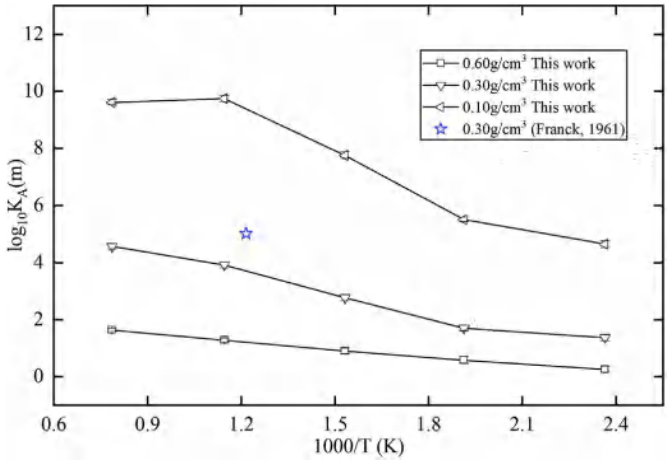

Fig. 5. log K_A(m) values of NaF at different conditions for "CIP + SIP" state.

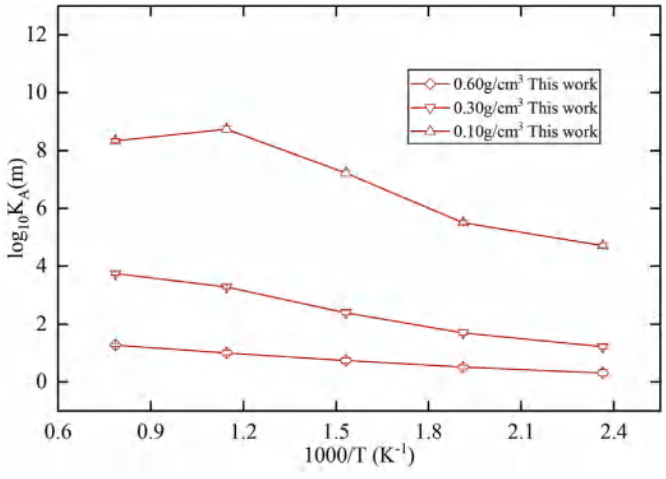

Fig. 6. log K_A(m) values of KF at different conditions for "CIP + SIP" state.

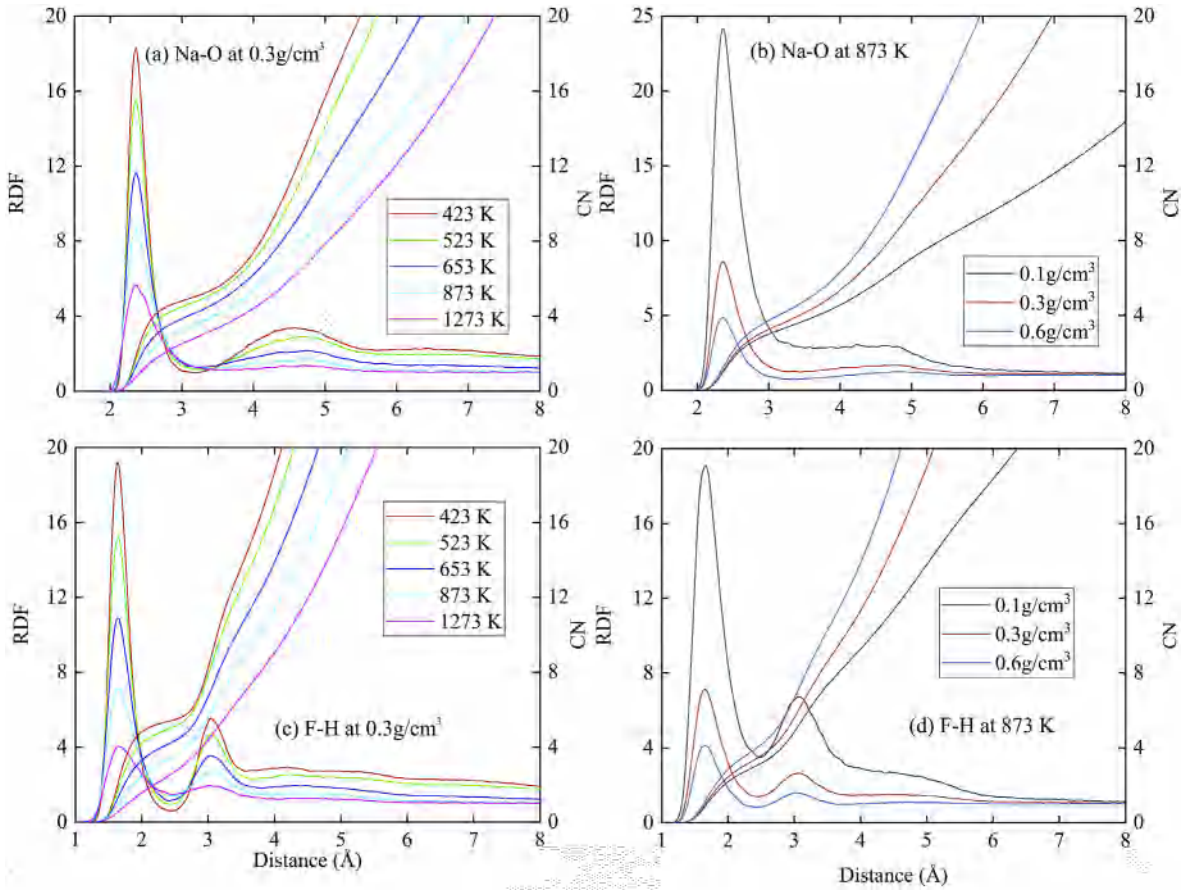

Fig. 7. The RDFs and CNs for Na-O and F-H at 0.30 g/cm^3 (**a**, **c**) and at 873 K (**b**, **d**). RDFs and CNs were denoted as identical color solid line corresponding to left-hand side and right-hand side vertical axes, respectively.

at 2.3, 4.6 and 6.2 Å respectively. For KF ion pair, the position of CIP is found around 2.8 because of the larger ionic size of K^+ than Na^+. It is observed that 2SIP is located at a fairly shallow trough, indicating that 2SIP is unfavorable. The first maxima are found around 3.0 Å and 3.4 Å for NaF and KF respectively, which are called transition state. The energy barriers from SIP to CIP are more than 1.5 kcal/mol, which is bigger than thermal energy kT, indicating it is difficult to spontaneously transform from SIP to CIP due to the high energy barrier at ambient conditions. The comparison of three minima suggests that SIP has the lowest energy indicating SIP is the most favorable ion pair type at ambient conditions. In the previous work, Fennell et al. found that SIP has the deepest well at ambient conditions for KF ion pair using the SPC/E water and OPLS ionic models [29], which is consistent with our result. But with TIP3P water and OPLS force field, their result showed that CIP is the most favorable ion pair type for NaF ion pair at ambient conditions [29]. This indicates that the models for ions and water can affect the depth of well and positions of different ion pair types.

Fig. 3 and Fig. 4 display the density dependence (left side) and temperature dependence (right side) of PMF curves for NaF and KF ion pairs, respectively. Herein, only the results at 873 K and 0.3 g/cm^3 were presented since PMF curves at high temperatures (423, 523, 653, 873, 1273 K) and low water densities (0.60, 0.30, 0.10 g/cm^3) conditions have similar shapes. The PMFs for NaF/KF ion pairs are characterized by one deep minimum followed by a shallow minimum, corresponding to the CIP state and SIP state respectively. However, 2SIP state appearing at ambient conditions is unimportant even disappears at higher temperatures. The positions of CIP minima for NaF/KF are around 2.3 Å and 2.8 Å at 653 K and 0.3 g/cm^3, which are consistent with the previous simulated values [39], 2.2 Å and 2.7 Å at 647 K and 0.322 g/cm^3, respectively. The minima for CIP and SIP are slightly different because of the selected ionic models. Note that the positions of first minima shift slightly towards shorter interionic distance with temperatures rising and water densities decreasing. With further increase of temperature or decrease of density, the second trough gradually changes into a broad platform, indicating that SIP state is not important at these conditions. At extremely high temperature (1273 K) and low density (0.10 g/cm^3), only one minimum is observed and the PMF curves become a deep valley, indicating that SIP is not favorable and only CIP can exist. Comparison of KF versus NaF ion pairs indicates that the association of NaF ion pair is stronger than that of KF ion pair.

Overall, CIP is the most stable and important state among three ion-pair states at high temperatures and low densities. SIP is metastable state in contrast to CIP. 2SIP is fairly unstable and provides a negligible contribution to ion pair association. With temperature increasing and water density decreasing, the energy barrier from SIP to CIP gradually decreases; at extremely high temperatures and low densities, only CIP can exist as associated ion pair.

3.2. Association constants

At the ambient conditions, the log K_A values of NaF ion pair are -1.74 ± 0.40 for CIP and -0.25 ± 0.26 for CIP + SIP. It is clear that

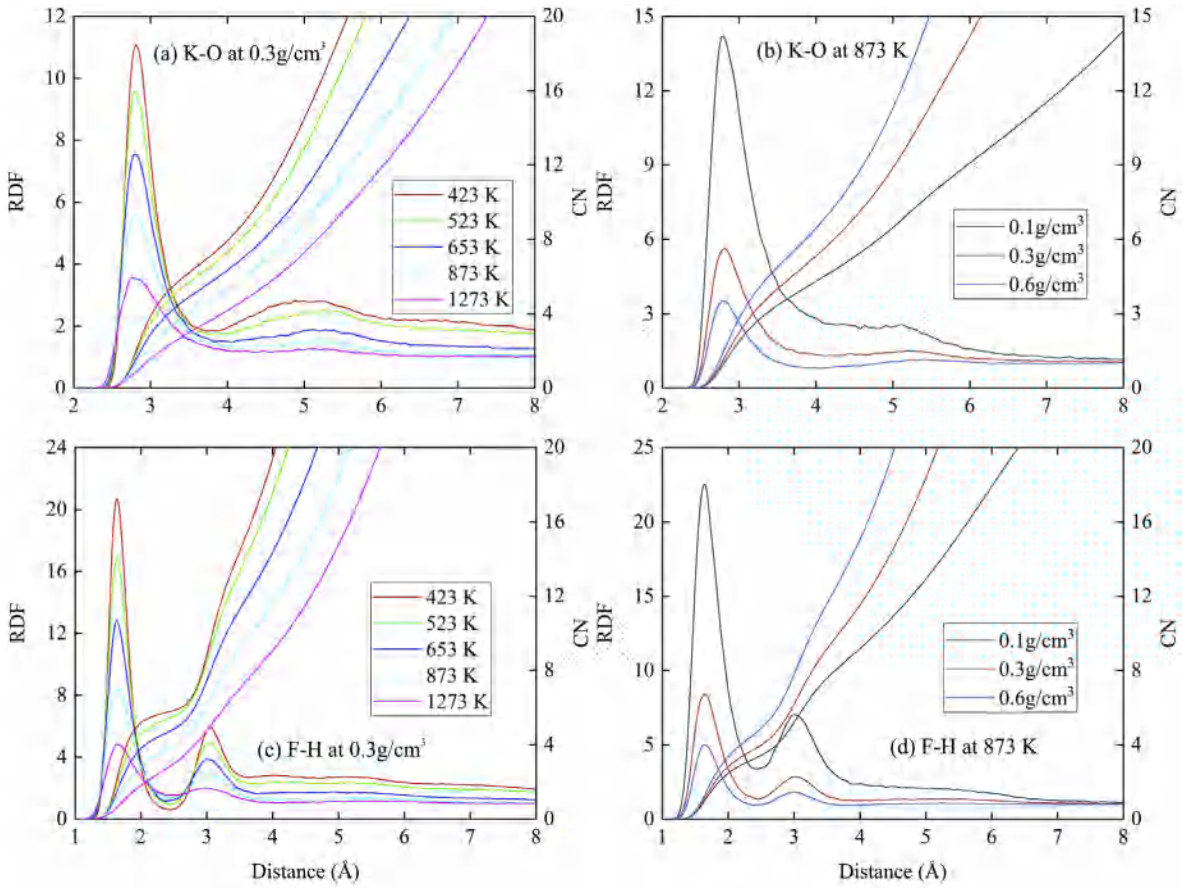

Fig. 8. The RDFs and CNs for K-O and F-H at 0.30 g/cm^3 (**a**, **c**) and at 873 K (**b**, **d**). RDFs and CNs were denoted as identical color solid line corresponding to left-hand side and right-hand side vertical axes, respectively.

the log K_A for CIP + SIP agrees with the experimental data of −0.38 [23], −0.78 [21] and −0.96 [19]. For KF ion pair, the calculated results at ambient conditions are −1.55 ± 0.37 for CIP and −0.10 ± 0.21 for CIP + SIP in favor of experimental value of −0.43 [20] and simulated value of −0.74 [29] for CIP. At higher temperatures, the log K_A(m) values of NaF and KF ion pairs are shown in Fig. 5 and Fig. 6, respectively. For NaF at 823 K and 0.30 g/cm^3, the calculated log K_A(m) value agrees with the experimental value within 1 logarithm unit [22]. In addition, the optimized potential models [37] (Joung and Cheatham models) with SPC/E water model were used to derive the association constants to compare with the Smith and Dang models with SPC/E water model. As depicted in Fig. S3, the two models show the same positions of CIP and SIP, while PMFs of the Smith and Dang models have a slightly deeper valley at CIP state than those of the Joung and Cheatham models. The evaluated log K_A(m) values at 653 K and 0.6 g/cm^3 are 0.90 ± 0.08 versus 0.75 ± 0.08 for Smith and Dang models and Joung and Cheatham models, respectively. It is clear that the two models give very similar results. At 873 K and 0.3/cm^3, the evaluated log K_A(m) values are 3.92 ± 0.10 versus 3.56 ± 0.08 for Smith and Dang models and Joung and Cheatham models, respectively. The result of Smith and Dang models is closer to the experimental value 5.0 at 823 K and 0.3 g/cm^3 [22]. These comparison further backups the models we employed.

Comparison between KF and NaF shows that the log K_A(m) values of NaF are similar to those of KF at low temperatures and high water densities but evidently larger at higher temperatures and lower densities, indicating that the association of NaF gets stronger as temperature increases and density reduces. Overall, the association constants increase with temperature increasing or density decreasing, implying that elevated temperature or decreased solvent density promotes the formation of ion pairs. Also, it was found that at low density (0.10 g/cm^3) and high temperature (873 K) association constants appeared to have a maximum. Up to now, few experimental association constants of NaF and KF can be used for comparison with our data at higher

Table 1
Coordination Numbers of the first coordination shell.

ion-water CNs	Temperature dependence (0.3 g/cm^3)					density dependence (873 K)		
	423 K	523 K	653 K	873 K	1273 K	0.1 g/cm^3	0.3 g/cm^3	0.6 g/cm^3
F-H (NaF)	5.4	5.0	4.2	3.5	2.6	3.1	3.5	4.0
F-H (KF)	5.8	5.5	4.7	3.9	3.0	3.3	3.9	4.5
Na-O	5.0	4.8	4.3	4.0	3.4	3.7	4.0	4.5
K-O	7.1	6.7	6.3	5.8	5.2	5.1	5.8	6.5

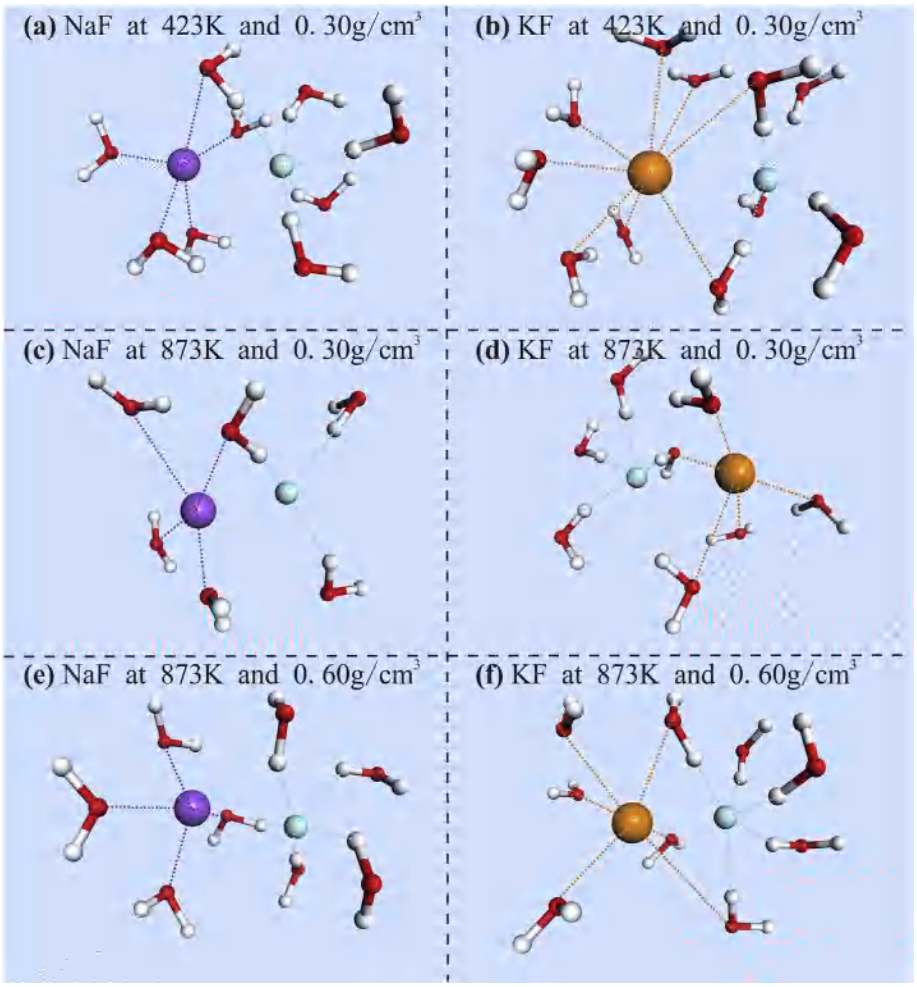

Fig. 9. The snapshots of hydration structures for NaF (**a**, **c** and **e**) and KF (**b**, **d** and **f**). For clarity, only ions and neighboring water molecules are displayed by ball and stick model. Coordination informations are indicated by different color dotted lines. Red = oxygen, white = hydrogen, purple = sodium, orange = potassium and cyan = fluorine.

temperatures except Ref. [22]. In the future, more modeling and experimental studies need to be done at high temperature to examine the accuracy of the reported K_A values in this work. The obtained association constant information can help us estimate the amount of NaF/KF ion pairs relative to free ions in hydrothermal fluids. Markedly, the higher values of log K_A(m) indicate the more considerable amount of ion pairs, especially existing in low-density steam phases containing abundant volatile components, which is likely to be a crucial role in controlling the mobility, transportation and enrichment of fluoride complexes.

To our knowledge, few association constants of K/NaF have been reported up to now especially at high temperatures. The derived data in this research can be used in future research on hydrothermal fluids, which is useful for understanding the transportation and migration of important metal ions in geological environment.

3.3. Ion pair structures and hydration structures

The M-O (M stands for Na/K) RDF and CN curves are showed in Fig. 7a,b and Fig. 8a,b, respectively. The first peaks of the Na-O RDFs are around 2.35 Å, close to 2.40 Å found in preceding works [50,51]. The first peaks of the K-O RDFs are around 2.80 Å. Table 1 shows the variation of CNs as temperature or density changes. When temperature increases from 473 K to 1273 K at a constant density (0.30 g/cm^3), the relevant CNs of Na-O change from 5.0 to 3.4 (Fig. 9a,c). Likewise, the CNs of K-O vary from 7.1 to 5.2 (Fig. 9b,d). At 653 K and 0.30 g/cm^3, the evaluated CN (4.2) for Na at CIP state is similar to the simulated value of 4.5 [39] but less than the single ion hydration number of 5.0 [36]. Comparison of CNs between Na^+ and K^+ suggests that K^+ has more coordinated water molecules than Na^+ at the same condition (Fig. 9a,b, c,d and e,f). Temperature dependence of CN data shows that the corresponding CNs only have slight variation as water density decreases (Fig. 9c,e and d,f), indicating that water molecule are inclined to gather around the K^+/Na^+ at high temperatures and low densities. This phenomenon has been reported in previous literatures and can be attributed to the enhancement of solute-solvent interaction compared to solvent-solvent interaction in supercritical fluids [48,52–55].

Fig. 7c,d and Fig. 8c,d display the F-H RDFs and CNs, which are indicative for hydrogen bonding. There are two pronounced peaks, which correspond to two hydrogen atoms in a water molecule. The first peak is centered at 1.60 Å, that is close to the previous MD simulation result of 1.55 Å [56]. The CNs of F-H (NaF) is slightly smaller than F-H (KF) at the same conditions, which closely relate to different hydration structures (Fig. 9c,d and e,f). With temperature increasing, the peak heights of F-H RDFs decrease dramatically and the relevant CNs reduce (Fig. 9a,c and b,d), suggesting the weakening of hydrogen bonding interaction. Water molecules

become less structured at higher temperatures. Hence, the charged ions are easier to associate.

4. Conclusions

In this work, classical MD technique has been employed to study KF/NaF ion pairs in water at high temperatures. The analyses of the PMFs suggest that CIP is the most stable configuration at high temperatures and low densities. The association constants derived from the PMFs show a rising trend as temperature increases or density decreases. The association of NaF is similar to KF under most conditions but evidently larger at higher temperatures and lower densities. The hydration structures of the ion pairs have been characterized in detail. It is found that water molecules gather around the K^+/Na^+ due to the stronger ion-water interaction compared to water-water interaction at high temperatures and low densities. The results indicate fluoride ion acts as an important ligand complexing with K^+/Na^+ in hydrothermal fluids.

CRediT authorship contribution statement

Xiaoyu Zhang: Conceptualization, Methodology, Software, Validation, Formal analysis, Investigation, Writing - original draft, Writing - review & editing, Visualization. **Xiandong Liu:** Conceptualization, Methodology, Resources, Writing - review & editing, Supervision, Project administration, Funding acquisition. **Mengjia He:** Methodology, Software, Formal analysis, Writing - review & editing, Visualization. **Yingchun Zhang:** Software, Resources, Writing - review & editing. **Yicheng Sun:** Formal analysis, Writing - review & editing. **Xiancai Lu:** Writing - review & editing, Supervision, Funding acquisition.

Acknowledgement

This study was supported by the National Key R&D Program of China (2018YFA0702700) and National Natural Science Foundation of China (No. 41572027, 41872041). We acknowledge supports from Newton International Fellowship Program and the State Key Laboratory for Mineral Deposits Research at Nanjing University. We are grateful to the High Performance Computing Center (HPCC) of Nanjing University for doing the numerical calculations in this paper on its blade cluster system.

Appendix A. Supplementary data

Supplementary data to this article can be found online at https://doi.org/10.1016/j.fluid.2020.112625.

List of symbols

Å	Angstrom (Å)
F	Average mean force (kcal mol^{-1} Å^{-1})
K_A	Association constants
K	Boltzmann constant (J K^{-1})
N_A	Avogadro constant
P	Pressure (Pa)
Q	Partial charge in units of $\|e\|$
r_{ij}	The separations of particles i and j (Å)
r_c	Cutoff distance (Å)
T	Temperature (K)
W	Potential energy (kcal mol^{-1})

Greek letters

ε	Lennard-Jones energy constant (kcal mol^{-1})
ε_0	Vacuum permittivity (C^2 N^{-1} m^{-2})
ϕ	Interaction energy (kcal mol^{-1})
π	Pi number
ρ	Density (g cm^{-3})
σ	Lennard-Jones length constant (Å)

Abbreviations

CIP	Contact ion pair
CN	Coordination number
LJ	Lennard-Jones
MD	Molecular dynamics
NVT	Ensemble: fixed number, volume and temperature
OPLS	Optimized potentials for liquid simulations
PMF	Potentials of mean force
RDF	Radial distribution function
SPC/E	Single point charge/extended
SIP	Solvent-shared ion pair
2SIP	Solvent-separated ion pair
TIP3P	Transferable intermolecular potential 3 points

Subscripts

i, j	Indexes of the interaction sites

Superscripts

+	Positive charge
−	Negative charge

References

[1] D.A.C. Manning, The effect of fluorine on liquidus phase-relationships in the system qz-ab-or with excess water at 1-kb, Contrib. Mineral. Petrol. 76 (1981) 206–215, https://doi.org/10.1007/bf00371960.
[2] A. Westland, Inorganic chemistry of the platinum-group elements, platinum-group elements: mineralogy, geology, recovery, CIM Spec. 23 (1981) 6–18.
[3] E.A. Mathez, J.D. Webster, Partitioning behavior of chlorine and fluorine in the system apatite-silicate melt-fluid, Geochem. Cosmochim. Acta 69 (2005) 1275–1286, https://doi.org/10.1016/j.gca.2004.08.035.
[4] J. Wu, K.T. Koga, Fluorine partitioning between hydrous minerals and aqueous fluid at 1 GPa and 770–947 C: a new constraint on slab flux, Geochem. Cosmochim. Acta 119 (2013) 77–92, https://doi.org/10.1016/j.gca.2013.05.025.
[5] A. Boudreau, I. McCallum, Investigations of the Stillwater Complex: Part V. Apatites as indicators of evolving fluid composition, Contrib. Mineral. Petrol. 102 (1989) 138–153, https://doi.org/10.1007/BF00375336.
[6] W.T. Chen, M.-F. Zhou, Mineralogical and geochemical constraints on mobilization and mineralization of rare Earth elements in the Lala Fe-Cu-(Mo, Ree) deposit, SW China, Am. J. Sci. 315 (2015) 671–711, https://doi.org/10.2475/07.2015.03.
[7] T. Hou, B. Charlier, O. Namur, P. Schütte, U. Schwarz-Schampera, Z. Zhang, F. Holtz, Experimental study of liquid immiscibility in the Kiruna-type Vergenoeg iron–fluorine deposit, South Africa, Geochem. Cosmochim. Acta 203 (2017) 303–322, https://doi.org/10.1016/j.gca.2017.01.025.
[8] Y. Xing, B. Etschmann, W. Liu, Y. Mei, Y. Shvarov, D. Testemale, A. Tomkins, J. Brugger, The role of fluorine in hydrothermal mobilization and transportation of Fe, U and REE and the formation of IOCG deposits, Chem. Geol. 504 (2019) 158–176, https://doi.org/10.1016/j.chemgeo.2018.11.008.
[9] J.F. Montreuil, E.G. Potter, L. Corriveau, W.J. Davis, Element mobility patterns in magnetite-group IOCG systems: the Fab IOCG system, Northwest Territories, Canada, Ore Geol. Rev. 72 (2016) 562–584, https://doi.org/10.1016/j.oregeorev.2015.08.010.
[10] D.J. Brabander, R.L. Hervig, D.M. Jenkins, Experimental determination of F- OH interdiffusion in tremolite and significance to fluorine-zoned amphiboles, Geochem. Cosmochim. Acta 59 (1995) 3549–3560, https://doi.org/10.1016/0016-7037(95)00222-L.
[11] Q. Duc-Tin, A. Audétat, H. Keppler, Solubility of tin in (Cl, F)-bearing aqueous fluids at 700 C, 140 MPa: a LA-ICP-MS study on synthetic fluid inclusions, Geochem. Cosmochim. Acta 71 (2007) 3323–3335, https://doi.org/10.1016/j.gca.2007.04.022.
[12] Y. Deng, D.K. Nordstrom, R.B. McCleskey, Fluoride geochemistry of thermal waters in Yellowstone National Park: I. Aqueous fluoride speciation, Geochem. Cosmochim. Acta 75 (2011) 4476–4489, https://doi.org/10.1016/j.gca.2011.05.028.
[13] B.O. Mysen, G.D. Cody, A. Smith, Solubility mechanisms of fluorine in peralkaline and meta-aluminous silicate glasses and in melts to magmatic temperatures, Geochem. Cosmochim. Acta 68 (2004) 2745–2769, https://doi.org/10.1016/j.gca.2003.12.015.
[14] C. Zhu, D.A. Sverjensky, F-Cl-OH partitioning between biotite and apatite, Geochem. Cosmochim. Acta 56 (1992) 3435–3467, https://doi.org/10.1016/

0016-7037(92)90390-5.
[15] A. Garand, A. Mucci, The solubility of fluorite as a function of ionic strength and solution composition at 25 C and 1 atm total pressure, Mar. Chem. 91 (2004) 27–35, https://doi.org/10.1016/j.marchem.2004.04.002.
[16] W. Zhang, L. Zhou, H. Tang, H. Li, W. Song, G. Xie, The solubility of fluorite in Na-K-Cl solutions at temperatures up to 260 C and ionic strengths up to 4 mol/kg H2O, Appl. Geochem. 82 (2017) 79–88, https://doi.org/10.1016/j.apgeochem.2017.04.017.
[17] C.K. Richardson, H. Holland, The solubility of fluorite in hydrothermal solutions, an experimental study, Geochem. Cosmochim. Acta 43 (1979) 1313–1325, https://doi.org/10.1016/0016-7037(79)90121-2.
[18] Y. Marcus, G. Hefter, Ion pairing, Chem. Rev. 106 (2006) 4585–4621, https://doi.org/10.1021/cr040087x.
[19] G.R. Miller, D.R. Kester, Sodium fluoride ion-pairs in seawater, Mar. Chem. 4 (1976) 67–82, https://doi.org/10.1016/0304-4203(76)90036-0.
[20] S. Manohar, G. Atkinson, The effect of high pressure on the ion pair equilibrium constant of alkali metal fluorides: a spectrophotometric study, J. Solut. Chem. 22 (1993) 859–872, https://doi.org/10.1007/BF00646598.
[21] A. Usha, G. Atkinson, The effect of pressure on the dissociation constant of hydrofluoric acid and the association constant of the NaF ion pair at 25° C, J. Solut. Chem. 21 (1992) 477–488, https://doi.org/10.1007/BF00649700.
[22] E. Franck, Überkritisches wasser als elektrolytisches lösungsmittel, Angew. Chem. 73 (1961) 309–322, https://doi.org/10.1002/ange.19610731003.
[23] E. Lukyanova, A. Zotov, Determination of the NaFaq association constant for the NaF–NaCl–H 2 O System at 25–75° C by means of potentiometry, Russ. J. Phys. Chem. 91 (2017) 672–677, https://doi.org/10.1134/S0036024417040148.
[24] C.E. Manning, Fluids of the lower crust: deep is different, Annu. Rev. Earth Planet Sci. 46 (2018) 67–97, https://doi.org/10.1146/annurev-earth-060614-105224.
[25] A.A. Chialvo, J.M. Simonson, Aqueous Na+Cl− pair association from liquidlike to steamlike densities along near-critical isotherms, J. Chem. Phys. 118 (2003) 7921–7929, https://doi.org/10.1063/1.1564052.
[26] K. Yui, M. Sakuma, T. Funazukuri, Molecular dynamics simulation on ion-pair association of NaCl from ambient to supercritical water, Fluid Phase Equil. 297 (2010) 227–235, https://doi.org/10.1016/j.fluid.2010.05.012.
[27] M. He, X. Liu, X. Lu, R. Wang, Molecular simulation study on K+–Cl− ion pair in geological fluids, Acta Geochem. 36 (2017) 1–8, https://doi.org/10.1007/s11631-016-0130-6.
[28] Z. Zhang, Z. Duan, Lithium chloride ionic association in dilute aqueous solution: a constrained molecular dynamics study, Chem. Phys. 297 (2004) 221–233, https://doi.org/10.1016/j.chemphys.2003.10.030.
[29] C.J. Fennell, A. Bizjak, V. Vlachy, K.A. Dill, Ion pairing in molecular simulations of aqueous alkali halide solutions, J. Phys. Chem. B 113 (2009) 6782–6791, https://doi.org/10.1021/jp908484v.
[30] L. Martínez, R. Andrade, E.G. Birgin, J.M. Martínez, PACKMOL: a package for building initial configurations for molecular dynamics simulations, J. Comput. Chem. 30 (2009) 2157–2164, https://doi.org/10.1002/jcc.21224.
[31] I.T. Todorov, W. Smith, K. Trachenko, M.T. Dove, DL_POLY_3: new dimensions in molecular dynamics simulations via massive parallelism, J. Mater. Chem. 16 (2006) 1911–1918, https://doi.org/10.1039/B517931A.
[32] H. Berendsen, J. Grigera, T. Straatsma, The missing term in effective pair potentials, J. Phys. Chem. 91 (1987) 6269–6271, https://doi.org/10.1021/j100308a038.
[33] S. Deublein, J. Vrabec, H. Hasse, A set of molecular models for alkali and halide ions in aqueous solution, J. Chem. Phys. 136 (2012), 084501, https://doi.org/10.1063/1.3687238.
[34] G.A. Orozco, O.A. Moultos, H. Jiang, I.G. Economou, A.Z. Panagiotopoulos, Molecular simulation of thermodynamic and transport properties for the H2O+NaCl system, J. Chem. Phys. 141 (2014) 234507, https://doi.org/10.1063/1.4903928.
[35] P.B. Balbuena, K.P. Johnston, P.J. Rossky, Molecular dynamics simulation of electrolyte solutions in ambient and supercritical water. 1. Ion solvation, J. Phys. Chem. 100 (1996) 2706–2715, https://doi.org/10.1021/jp952194o.
[36] J.C. Rasaiah, J.P. Noworyta, S. Koneshan, Structure of aqueous solutions of ions and neutral solutes at infinite dilution at a supercritical temperature of 683 K, J. Am. Chem. Soc. 122 (2000) 11182–11193, https://doi.org/10.1021/ja001978z.
[37] I.S. Joung, T.E. Cheatham, Determination of alkali and halide monovalent ion parameters for use in explicitly solvated biomolecular simulations, J. Phys. Chem. B 112 (2008) 9020–9041, https://doi.org/10.1021/jp8001614.
[38] A. Plugatyr, I.M. Svishchev, Accurate thermodynamic and dielectric equations of state for high-temperature simulated water, Fluid Phase Equil. 277 (2009) 145–151, https://doi.org/10.1016/j.fluid.2008.12.003.
[39] A. Sarkar, B.L. Tembe, Molecular dynamics simulations of alkali metal halides in supercritical water, Chem. Phys. Lett. 639 (2015) 71–77, https://doi.org/10.1016/j.cplett.2015.08.032.
[40] L.X. Dang, Development of nonadditive intermolecular potentials using molecular dynamics: solvation of Li+ and F− ions in polarizable water, J. Chem. Phys. 96 (1992) 6970–6977, https://doi.org/10.1063/1.462555.
[41] D.E. Smith, L.X. Dang, Computer simulations of NaCl association in polarizable water, J. Chem. Phys. 100 (1994) 3757–3766, https://doi.org/10.1063/1.466363.
[42] J.-P. Ryckaert, G. Ciccotti, H.J. Berendsen, Numerical integration of the cartesian equations of motion of a system with constraints: molecular dynamics of n-alkanes, J. Comput. Phys. 23 (1977) 327–341, https://doi.org/10.1016/0021-9991(77)90098-5.
[43] D. Fincham, Leapfrog rotational algorithms, Mol. Simulat. 8 (1992) 165–178, https://doi.org/10.1080/08927029208022474.
[44] M.P. Allen, D.J. Tildesley, Computer Simulation of Liquids, Oxford university press, 2017.
[45] S. Nosé, A molecular dynamics method for simulations in the canonical ensemble, Mol. Phys. 52 (1984) 255–268, https://doi.org/10.1080/00268970110089108.
[46] W.G. Hoover, Canonical dynamics: equilibrium phase-space distributions, Phys. Rev. 31 (1985) 1695, https://doi.org/10.1103/PhysRevA.31.1695.
[47] M.C. Justice, J.C. Justice, Ionic interactions in solutions. I. The association concepts and the McMillan-Mayer theory, J. Solut. Chem. 5 (1976) 543–561, https://doi.org/10.1007/BF00647377.
[48] J. Gao, Simulation of the Na+ Cl-ion pair in supercritical water, J. Phys. Chem. 98 (1994) 6049–6053, https://doi.org/10.1021/j100075a001.
[49] W. Liu, R.H. Wood, D.J. Doren, Hydration free energy and potential of mean force for a model of the sodium chloride ion pair in supercritical water with ab initio solute–solvent interactions, J. Chem. Phys. 118 (2003), https://doi.org/10.1063/1.1536164.
[50] T. Ikeda, M. Boero, Communication: hydration structure and polarization of heavy alkali ions: a first principles molecular dynamics study of Rb+ and Cs+, J. Chem. Phys. (2012) https://doi.org/10.1063/1.4742151. In AIP.
[51] A. Bankura, V. Carnevale, M.L. Klein, Hydration structure of salt solutions from ab initio molecular dynamics, J. Chem. Phys. 138 (2013), 014501, https://doi.org/10.1063/1.4772761.
[52] P.G. Debenedetti, R.S. Mohamed, Attractive, weakly attractive, and repulsive near-critical systems, J. Chem. Phys. 90 (1989) 4528–4536, https://doi.org/10.1063/1.456639.
[53] I.B. Petsche, P.G. Debenedetti, Solute–solvent interactions in infinitely dilute supercritical mixtures: a molecular dynamics investigation, J. Chem. Phys. 91 (1989) 7075–7084, https://doi.org/10.1063/1.457325.
[54] P. Cummings, H. Cochran, J. Simonson, R. Mesmer, S. Karaborni, Simulation of supercritical water and of supercritical aqueous solutions, J. Chem. Phys. 94 (1991) 5606–5621, https://doi.org/10.1063/1.460497.
[55] T.A. Betts, J. Zagrobelny, F.V. Bright, Spectroscopic determination of solute-fluid cluster size in supercritical nitrogen oxide (N2O), J. Am. Chem. Soc. 114 (1992) 8163–8171, https://doi.org/10.1021/ja00047a027.
[56] A. Chaumont, G. Wipff, Halide anion solvation and recognition by a macrotricyclic tetraammonium host in an ionic liquid: a molecular dynamics study, New J. Chem. 30 (2006) 537–545, https://doi.org/10.1039/B518109G.